

Analysis of hollow-core slab floors

P.C.J. Hoogenboom

Delft University of Technology, Faculty of Civil Engineering and Geosciences, Delft, The Netherlands

This paper provides a procedure for finite element analysis of hollow-core slab floors, which may be necessary in case of large floor openings. Formulas for homogenisation of the floor properties are presented. Finite element modelling is discussed. Formulas for stress recovery are presented. As an example a floor is analysed with a 3×3.6 m opening.

Key words: Hollow-core slabs, trimmer, homogenisation, stress recovery, analysis procedure

1 Introduction

Openings in hollow-core slab floors occur often. The short slabs are supported by a trimmer that is supported by the adjacent continuing slabs (Fig. 1). Special calculations are not required if the opening has a size of one or two times the slab width. However, sometimes larger openings are needed, for example for large flight of stairs. These openings are preferably constructed without expensive and obstructive support structure. The strength and stiffness of such a design can be determined by linear elastic finite element analyses for which this paper presents a practical procedure.

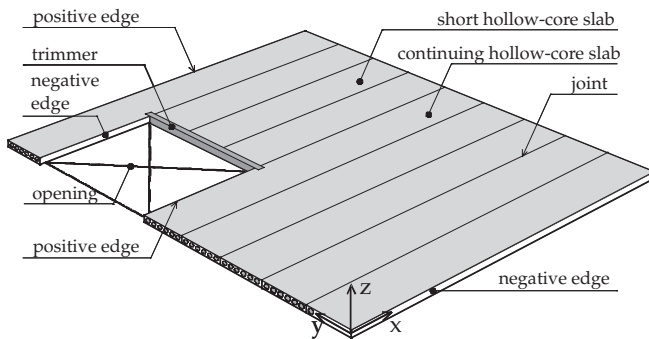


Figure 1: A large opening in a hollow-core slab floor

A computational method for homogenisation of plate stiffness properties has been developed by A. Kok [Kok 2002]. It has been successfully applied to hollow-core slab floors. However, this method does not provide a way to check whether the computed section moments and section

forces exceed the floor capacity. Therefore, in the present paper a method is proposed to calculate the stresses that are caused by the section moments and section forces in critical points of a floor. This is referred to as stress recovery. Subsequently, these stresses are checked against the material strengths.

2 Finite element modelling

The stresses in a hollow-core slab floor depend on the way the floor is constructed. In the beginning of construction the slab joints are not filled and the slabs are mainly loaded by self-weight. The prestressing force is already present and one or more trimmers carry the loading of the short slabs to the continuing slabs. Subsequently, when the joints have been filled and cured, the live load is applied. The live load is distributed over multiple slabs by the joints. Therefore, the floor has two stiffnesses, a stiffness without the joints and a stiffness with the joints.

At first sight a non-linear analysis seems to be necessary to account for the changing stiffness. However, since the stiffness does not depend on the deformation or the loading the analysis can be performed by two linear elastic finite element computations. In the first analysis the joints are left out and the floor is loaded by self-weight and prestress only. In the second analysis the joints are filled and the floor is loaded by the live load only. Subsequently, the loading, displacements and sections forces of the two computations are superposed. (Fig. 2).

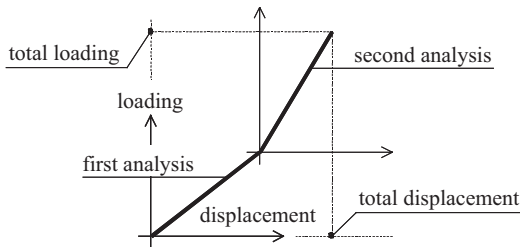


Figure 2: Computation of a hollow-core slab floor in two steps

The finite element model consists of plate elements and beam elements. The plate elements have to be approximately as wide as the center-to-center distance of the channels. The length of the elements is approximately the thickness of the slab. At the support of the trimmer the elements need to be as long as the width of the support platen. Smaller elements are inconvenient because they would show peaks in the force flow that do not occur in reality. These peaks occur because the plate theory is not accurate near concentrated loading that occurs due to the trimmer ends. The trimmer is modelled with beam elements. The joints are also modelled with plate elements, which are as wide as the joints, for example 30 mm.

3 Homogenisation of the slab properties

Hollow-core slab plates can be modelled as orthotropic plates using the Reissner-theorie. We choose the x -axis in the direction of the channels and the z -axis upwards. In this case the following set of constitutive equations holds

$$\begin{aligned}
 m_{xx} &= \frac{E}{(1-\nu^2)}(I_x \kappa_{xx} + \nu I_y \kappa_{yy}) \\
 m_{yy} &= \frac{E}{(1-\nu^2)}I_y(\kappa_{yy} + \nu \kappa_{xx}) \\
 m_{xy} &= G I_t \kappa_{xy} \\
 q_x &= G \eta_x A_x \phi_x \\
 q_y &= G \eta_y A_y \phi_y,
 \end{aligned} \tag{1}$$

where E , G and ν are Young's modulus, the shear modulus and Poisson's ratio.

$m_{xx}, m_{yy}, m_{xy}, q_x, q_y$ are section forces per unit of length as drawn in Figure 3. $\kappa_{xx}, \kappa_{yy}, \kappa_{xy}$ are curvatures and ϕ_x, ϕ_y are shear deformations. If the channel cross-sections are approximated by a rectangular shape (Fig. 3) the following plate properties can be derived [Span 2002].

The area per unit length of a section in the y -direction is

$$A_x = t_1 + t_2 + a. \tag{2}$$

where $a = \frac{t_3}{b_1}(h - t_1 - t_2)$ is the area of the flange. The moment of inertia per unit length of this section is

$$\begin{aligned}
 I_x &= \frac{1}{12}t_1^3 + t_1(z_x - \frac{1}{2}t_1)^2 + \frac{1}{12}t_2^3 + t_2(h - z_x - \frac{1}{2}t_2)^2 + \\
 &\quad + \frac{1}{12}a(h - t_1 - t_2)^2 + a(z_x - \frac{1}{2}(h + t_1 - t_2))^2,
 \end{aligned} \tag{3}$$

where $z_x = \frac{S_x}{A_x}$ and $S_x = \frac{1}{2}t_1^2 + a\frac{1}{2}(h + t_1 - t_2) + t_2(h - \frac{1}{2}t_2)$.

The area per unit length of a section in the x -direction is

$$A_y = t_1 + t_2. \tag{4}$$

The moment of inertia per unit length of this section is

$$I_y = \frac{1}{12}t_1^3 + t_1(z_y - \frac{1}{2}t_1)^2 + \frac{1}{12}t_2^3 + t_2(h - z_y - \frac{1}{2}t_2)^2, \tag{5}$$

where $z_y = \frac{S_y}{A_y}$ and $S_y = \frac{1}{2}t_1^2 + t_2(h - \frac{1}{2}t_2)$.

The torsion constant is

$$I_t = \frac{t_1 t_2 (2h - t_1 - t_2)^2}{4(t_1 + t_2)} \quad (6)$$

The shape factor for the shear stiffness in the x -direction is

$$\eta_x = \frac{h - \frac{1}{2}(t_1 + t_2)}{h + (\frac{b_1}{t_3} - 1)(t_1 + t_2)} \quad (7)$$

The shape factor for the shear stiffness in the y -direction is

$$\eta_y = \frac{2t_3^3}{b_1 c (t_1 + t_2)(1 - \nu)} \frac{12 + \xi}{12 + 4\xi + \zeta} \quad (8)$$

where $c = 2h - t_1 - t_2$, $\xi = \frac{b_1(t_1^3 + t_2^3)t_3^3}{c t_1^3 t_2^3}$ and $\zeta = \frac{b_1^2 t_3^6}{c^2 t_1^3 t_2^3}$.

The joints usually are of poor concrete quality and not reinforced. Therefore, a joint can crack in the longitudinal direction. This causes a hinging connection between the slabs¹. Therefore, the joints are modelled with a material that has no bending stiffness in lateral direction²

$$I_y = 0 \quad (9)$$

The other stiffness properties of the joints can be the same as those of the hollow core slabs. Actually, this is not correct because the joints are solid while the slabs are hollow. However, the effect of the thin joints on the force flow in the floor is negligible. The advantages are that less typing is needed to prepare the program input and no peaks in the shear force occur, which makes it easier to interpret the computational results.

1 Floors often have edge reinforcement. Therefore, the slabs cannot shift when rotation in a joint occurs. As a consequence, the joint can carry a transverse moment. Unfortunately, it is not easy to quantify this situation. Therefore, the joints are conservatively modelled as perfect hinges.

2 Instead of joint elements it is also possible to leave out these elements and connect the vertical displacements of the slab edges by tyings. However, this cannot be realised easily in many finite element programs.

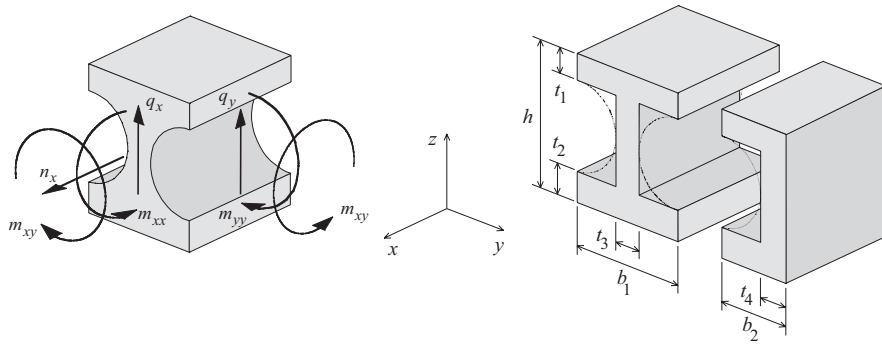


Figure 3: Section forces and approximated representative volume of a hollow-core slab

4 Recovery of stresses

The section forces are computed by a finite element program, for example KOLA [Lamers 1995]. Obviously the section forces cause stresses in the material of the hollow-core slab. The distribution of these stresses can be estimated with some accuracy. (Fig. 4).

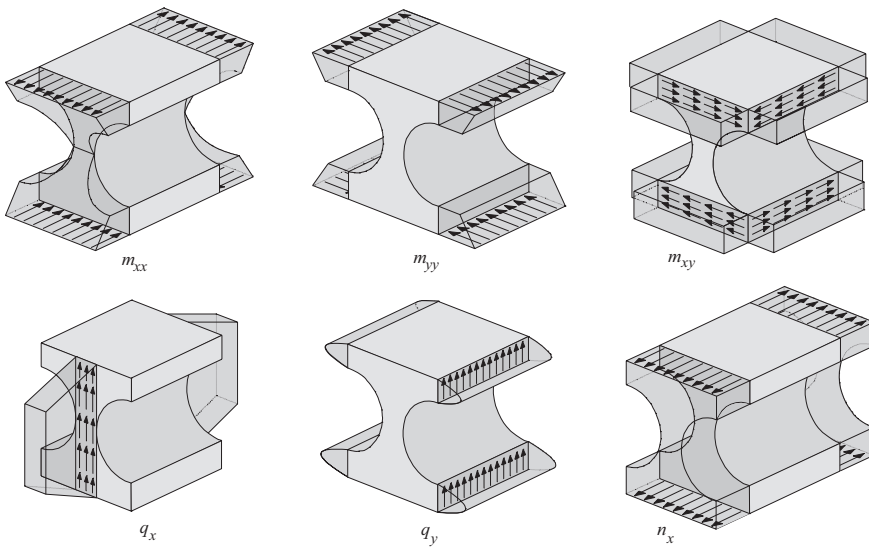


Figure 4: Approximated stress distributions in a representative volume of a hollow-core slab

From the stress distributions the stress in the middle of the top flange can be derived (Fig. 5).

$$\begin{aligned}
 \sigma_{xx} &= \frac{m_{xx}}{I_x} \left(z_x - \frac{1}{2} t_1 \right) + \frac{n_x}{A_x} \\
 \sigma_{yy} &= \frac{m_{yy}}{I_y} \left(z_y - \frac{1}{2} t_1 \right) \\
 \sigma_{xy} &= \frac{2m_{xy}}{t_1 (2h - t_1 - t_2)} \\
 \sigma_{yz} &= \frac{3}{2} \frac{t_1^2 q_y}{t_1^3 + t_2^3}
 \end{aligned} \tag{10}$$

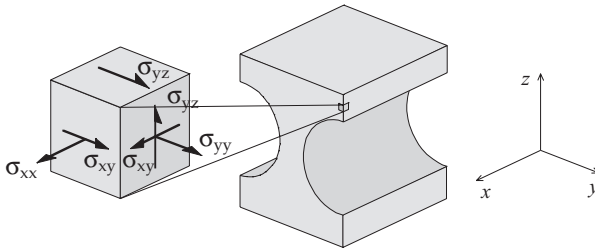


Figure 5: Stress state in the middle of the top flange

The stresses that are not mentioned are equal to zero. The stress state in the middle of a web is (Fig. 6).

$$\begin{aligned}
 \sigma_{xx} &= \frac{n_x}{A_x} \\
 \sigma_{yz} &= \frac{3b_1 t_2 \left(h - z_y - \frac{1}{2} t_2 \right) q_y}{2t_3 I_y} \\
 \sigma_{zx} &= \frac{2b_1 q_x}{t_3 (2h - t_1 - t_2)}
 \end{aligned} \tag{11}$$

The latter formulas are valid for the interior of a floor. At a supported or free edge other formulas hold. In this we distinguish between positive and negative edges. An edge is positive if the outward directed normal vector points in the direction of the y -axis. An edge is negative if this normal vector points in the opposite direction of the y -axis (Fig. 1). The stress state in the middle of a web of a positive edge is

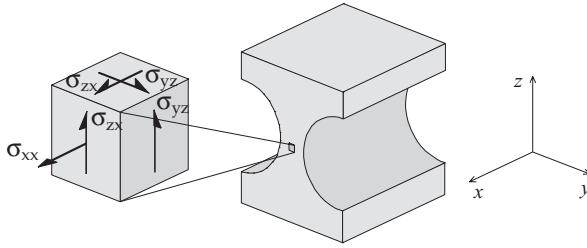


Figure 6: Stress state in a web

$$\begin{aligned}
 \sigma_{xx} &= \frac{n_x}{A_x} \\
 \sigma_{yz} &= \frac{3b_2t_2(h-z_y - \frac{1}{2}t_2)q_y}{2t_4I_y} \\
 \sigma_{zx} &= 2 \frac{b_2q_x - m_{xy}}{t_4(2h-t_1-t_2)}
 \end{aligned} \tag{12}$$

For negative edges it holds

$$\begin{aligned}
 \sigma_{xx} &= \frac{n_x}{A_x} \\
 \sigma_{yz} &= \frac{3b_2t_2(h-z_y - \frac{1}{2}t_2)q_y}{2t_4I_y} \\
 \sigma_{zx} &= 2 \frac{b_2q_x + m_{xy}}{t_4(2h-t_1-t_2)}
 \end{aligned} \tag{13}$$

The stress distribution at the supports of the slabs cannot be determined with a simple formula. However, experiments show that in practical situations failure does not occur at the supports [Aswad 1992]. From the stresses the principal stresses are calculated. These are the eigenvalues of the matrix

$$\begin{bmatrix}
 \sigma_{xx} & \sigma_{xy} & \sigma_{zx} \\
 \sigma_{xy} & \sigma_{yy} & \sigma_{yz} \\
 \sigma_{zx} & \sigma_{yz} & \sigma_{zz}
 \end{bmatrix} \tag{14}$$

The plate stiffnesses are calculated using Eq. 2 to 8.

$$\begin{aligned} I_x &= 4.80 \cdot 10^{-4} \text{ m}^3 & \eta_x A_x &= 313.16 \cdot 10^{-4} \text{ m} \\ I_y &= 4.38 \cdot 10^{-4} \text{ m}^3 & \eta_y A_y &= 10.82 \cdot 10^{-4} \text{ m} \\ I_t &= 4.34 \cdot 10^{-4} \text{ m}^3 \end{aligned}$$

The support area of the trimmer is 0.15 m wide. The trimmer has the following moments of inertia.

$$\begin{aligned} I_x &= 65.06 \cdot 10^{-6} \text{ m}^4 \\ I_t &= 0.82 \cdot 10^{-6} \text{ m}^4 \end{aligned}$$

The finite element program KOLA computes the deformation and the force flow in the floor (Fig. 10, 11). In the first analysis the slabs are not connected and the plate is loaded by self-weight only. The prestress loading is calculated manually. In the second analysis the joints are connected by hinges and the plate is loaded by live load only. In eight elements the stresses are checked. These elements have a dark grey colour in Figure 7. The stresses are checked at some distance of the slab support because there the prestress is completely developed. The Appendix shows the average section forces of the eight elements. The moments in the continuing slab are smaller than the moment capacity of the cross-section ($| -104 \text{ kNm} | < | -143 / 1.2 |$).

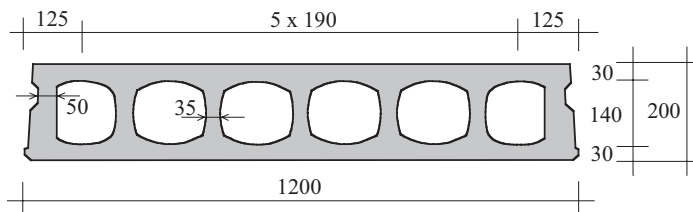


Figure 8: Cross-section of hollow-core slab N200

Subsequently, the local stress state is computed in the flanges, webs and edges using Eq. 10 to 13 (Table 1). It is shown that largest tensile stress (1.98 MPa) occurs in the web at the location of element 2895. This is smaller than the design value of the concrete tensile strength (2.10 MPa). All compressive stresses are sufficiently small. Consequently the floor design is sufficient. The floor is loaded up to 94% of its capacity.

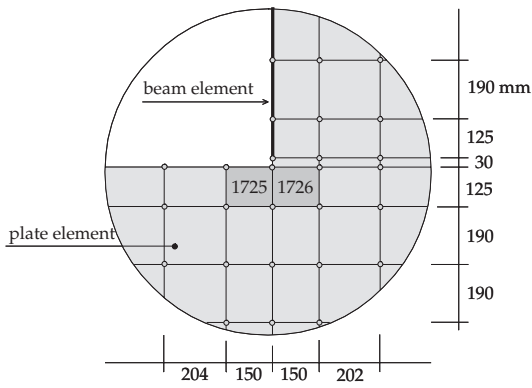


Figure 9: Detail of a re-entrant corner of the element mesh

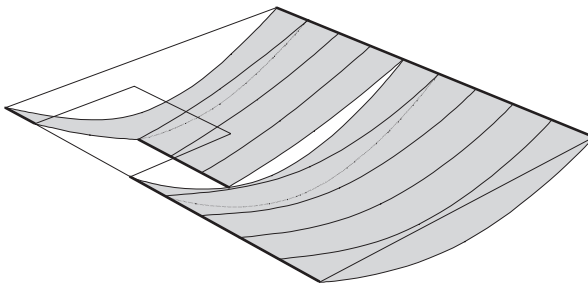


Figure 10: Deformation of the floor due to self-weight in step 1 of the analysis

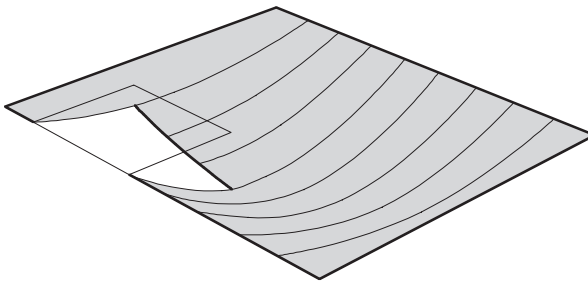


Figure 11: Deformation of the floor due to live load only in step 2 of the analysis

Table 1: Principal stresses [MPa] in the elements of Figure 7

element number	top flange		web or edge	
	largest principal stress	smallest principal stress	largest principal stress	smallest principal stress
1688	0.17	-13.99	0.21	-6.92
1712	0.19	-4.07	0.54	-7.40
1725	0.81	-25.41	1.31	-7.53
1726	1.50	-21.00	1.43	-6.97
2882	0.51	-6.54	1.45	-8.28
2895	0.91	-15.73	1.98	-8.61
2896	1.17	-13.99	1.25	-6.91
2948	0.09	-10.47	0.15	-6.90

6 Conclusions

A method has been presented for finite element analysis of hollow-core slab floors. The method includes formulas for homogenisation of the slab properties and formulas for stress recovery. The principal stresses are calculated and checked at critical locations of the floor.

It is shown that large openings in hollow-core slab floors can be possible without extra beams or columns. The proposed method is a practical way to check the floor capacity.

It is planned to develop a program for analysis of hollow core slab floors based on the procedure presented in this paper. The program will do the finite element modelling, structural analysis and stress recovery. Therefore, the structural designer will just need to enter the floor geometry and loading after which the program computes the largest stress. It is expected that this program will be a useful design tool.

References

- Kok, A.W.M. (2002) Artificial Orthotropy, *HERON*, Vol. 47, No. 1, pp. 29-51.
- Span, L. (2002) Large Openings in Hollow-Core Slab Floors, (Grote openingen in kanaalplaatvloeren), MSc report *Delft University of Technology* (in Dutch).
- Lamers (1995) *Users Guide of KOLA*, Ingenieursbureau Lamers, Naaldwijk.
- Dycore (2001) *Dycore Systeenvloeren*, Zekerheid als basis, Productinformatie (In Dutch).
- Aswad, A., F.J. Jacques (1992) Behavior of Hollow-Core Slabs Subjected to Edge Loads, *PCI Journal*, Vol 37, No 2, p. 72-84.

Appendix

Moments [kNm/m] en forces [kN/m] in eight critical elements

1688	self-weight	prestress	live load	total
mxx	-54.099	41.420	-26.820	-39.499
myy	0.064		-0.105	0.041
mxy	-2.014		-4.156	-6.170
qx	7.931		4.394	12.325
qy	-0.249		4.404	4.155
nx		-591.670		-591.670
1712	self-weight	prestress	live load	total
mxx	-12.196	41.420	-12.462	16.762
myy	-0.165		-0.227	-0.392
mxy	1.746		2.133	3.879
qx	-49.214		-51.558	-100.772
qy	2.578		3.468	6.046
nx		-591.670		-591.670
1725	self-weight	prestress	live load	total
mxx	-65.009	41.420	-80.30	-103.889
myy	1.432		-5.819	-4.387
mxy	1.270		-10.092	-8.822
qx	-90.410		-127.901	-218.311
qy	-21.328		-23.616	-44.944
nx		-591.670		-591.670
1726	self-weight	prestress	live load	total
mxx	-62.960	41.420	-55.032	-76.572
myy	1.517		-0.357	1.160
mxy	-2.057		-15.333	-17.390
qx	104.122		-72.254	31.868
qy	-18.708		-23.523	-42.231
nx		-591.670		-591.670

2882	self-weight	prestress	live load	total
mxx	-12.196	41.420	-24.728	4.496
myy	-0.165		-0.773	-0.938
mxy	-1.753		-6.742	-8.495
qx	-49.271		-112.959	-162.230
qy	-2.583		-12.327	-14.910
nx		-591.670		-591.670
2895	self-weight	prestress	live load	total
mxx	-64.901	41.420	-26.289	-49.770
myy	1.436		-1.753	-0.317
mxy	-1.289		-1.694	-2.983
qx	-90.773		-145.013	-235.786
qy	21.415		15.880	37.295
nx		-591.670		-591.670
2896	self-weight	prestress	live load	total
mxx	-62.877	41.420	-18.466	-39.923
myy	1.522		0.489	2.011
mxy	2.050		1.094	3.144
qx	103.909		-91.425	12.484
qy	18.828		18.614	37.442
nx		-591.670		-591.670
2948	self-weight	prestress	live load	total
mxx	-53.952	41.420	-7.298	-19.830
myy	0.065		-0.292	-0.227
mxy	2.025		2.014	4.039
qx	7.932		-2.907	5.025
qy	0.257		2.955	3.212
nx		-591.670		-591.670